NASA TECHNICAL MEMORANDUM

NASA TM X- 62,388

NASA TM X- 62,388

(NASA-TM-X-62388) SEISMIC EFFECTS FROM MAJOR BASIN FORMATION ON THE MOON AND MERCURY (NASA) 41 p HC 3.25 CSCL 03B

N74-34281

Unclas
G3/30 49322

SEISMIC EFFECTS FROM MAJOR BASIN FORMATION ON THE MOON AND MERCURY

Peter H. Schultz and Donald E. Gault

Ames Research Center
Moffett Field, California 94035

September 1974

Abstract

Grooved and hilly terrains occur at the antipode of major basins on the Moon (Imbrium, Orientale) and Mercury (Caloris). Such terrains may represent extensive landslides and surface disruption produced by impact-generated P waves and antipodal convergence of surface waves. Order-of-magnitude calculations for an Imbrium-size impact (10^{34} ergs) on the Moon indicate P-wave-induced surface displacements of 10 m at the basin antipode that would arrive prior to secondary ejecta. Comparable surface waves would arrive subsequent to secondary ejecta impacts beyond 10^{3} km and would increase in magnitude as they converge at the antipode. Other seismically induced surface features include: subdued, furrowed crater walls produced by landslides and concomitant secondary impacts; emplacement and leveling of light plains units owing to seismically induced "fluidization" of slide material; knobby, pitted terrain around old basins from enhancement of seismic waves in ancient ejecta blankets; and perhaps the production and enhancement of deep-seated fractures that led to the concentration of farside lunar maria in the Apollo-Ingenii region.

Seismic Effects from Major Basin Formation on the Moon and Mercury

by

Peter H. Schultz

and

Donald E. Gault

Space Science Division, NASA Ames Research Center

Moffett Field CA 94035

Introduction

Recently, the remarkable images from Mariner 10 disclosed a hilly and lineated terrain on Mercury that occurs antipodal to the 1300 km diameter Caloris Basin (Murray et al., 1974). Moore et al. (1974) and Schultz (1974) have recognized a similar extensively grooved lunar terrain antipodal to the Imbrium Basin. Moore et al. attributed the terrain to clustering of basin-related secondary impacts at the antipode. Schultz (1972, 1974), however, suggested that it indicates extensive mass wasting by seismic events and, in particular, that it may have resulted from antipodal enhancement of seismic waves generated by the enormous Imbrium event. In addition, highly complex terrains characterized by grooves, furrows, pits, and hills occur around old lunar basins (Eggleton and Marshall, 1962, Titley and Eggleton, 1964; Trask and Titley, 1966; Wilhelms and McCauley, 1971) and have been interpreted as volcanically modified basin ejecta (Wilhelms and McCauley, 1971) and furrowing and pitting by secondary ejecta (Howard, 1974). This paper explores some aspects of a seismic origin for such terrains, and in particular the complex antipodal regions.

Descriptions of Antipodal Terrains

Figure 1a shows the grooved terrain near the Mare Ingenii region on the Moon (160^{O}E, -34^{O}) which is antipodal to the Imbrium Basin (20^{O}W, $+35^{O}$). Wide grooves extend down the inner wall and outer rim of the Ingenii Basin as well as other sloped surfaces. Numerous smaller craters exhibit furrowed and relatively smooth walls without well-preserved slump blocks, yet in several examples the crested rim profile has been preserved. Light plains units commonly, but not exclusively, occur within these craters. Similar units also occur in smaller patches within the intercrater areas, which generally are characterized by numerous small hills, pits, and chaotic texture. Figure 1b illustrates the furrowed terrain adjacent to Mare Marginis (85^{O}E, $+15^{O}$), which is approximately antipodal to the Orientale Basin (95^{O}W, -20^{O}). The gross regional morphology is similar to that shown in Figure 1a.

The features illustrated by Figure 1 suggest a sudden catastrophic mode of degradation. Long-term processes, such as meteoroid erosion and deposition, are inconsistent with the preservation of both the crested rim profiles and the relatively small scale features (the small hills, pits, and surface textures). Encroachment of these features by mare units indicate that the catastrophism must predate the last stages of mare flooding, consistent with a genetic relation to the formation of the major basins.

Figure 2 shows the hilly and lineated terrain on Mercury from Mariner 10. The descriptions given by Murray et al. (1974) are similar to those for the regions shown in Figure 1. It covers a wide region (5×10^{5} km^{2}) that is antipodal to the enormous Caloris Basin, approximately 1300 km in diameter. Murray et al. (1974) conclude that the terrain developed over a long period of time because craters of similar sizes within this region appear to exhibit different states of modification. As a result, they suggest a volcanic origin.

However, the existence of different modification states can reflect catastrophic alteration of craters having different precatastrophe states of preservation. Moreover, heavily modified craters can be rejuvenated in appearance by subsequent processes, such as landslides, which can reestablish a subdued but scarplike (under low solar illumination) crater wall. Additionally, postcatastrophism impact craters forming after the knobby terrain can exhibit a rim facies that appears degraded relative to rim facies of craters formed in plains regions. This latter possibility is well illustrated by comparison between lunar craters formed in the highlands and those formed in the maria; it is particularly evident where resolution is poor and illumination angle is low, as exhibited in certain Mariner 10 images.

Areas having similar surface expressions but not antipodal to recent lunar basins also occur near the Sirsalis Rille on the edge of the Orientale ejecta blanket (60^{o}W, -10^{o}) and near the Apollo 16 landing site (15^{o}E, -10^{o}); the possible relationships of these sites to basin formation will be examined below.

Theoretical Calculations

An order-of-magnitude estimate of seismically induced surface displacements can be made by adapting a simple model described by Rinehart (1960). The seismic energy generated by an impact is assumed to be distributed in a pulse of length λ and initial peak stress σ_o. In passing through the body, the magnitude of the P wave dissipates geometrically and reflects as a tension wave at the antipodal surface, accelerating the free surface vertically to twice the particle velocity in the wave. For simplicity, a saw-toothed profile of the stress-time plot is assumed in which the pulse front contains the maximum stress with a linearly decreasing stress along the length of the pulse. Rinehart has shown that the maximum stress, σ_o is related to the

total kinetic energy, E, of this pulse by the following relation:

(1) $$\sigma_o^2 = \frac{6E\rho c}{At_o}$$

where ρ is the density, c is the wave velocity, A is the surface area of the wavefront, and t_o is the time length of the pulse. If it is assumed that the initial wavefront corresponds to the effective radius (r_o) of the incipent crater and that the kinetic energy of the wave is simply the the seismic energy (E_s). then equation (1) can be expressed in terms of the impact energy, E_T, by

(2) $$\sigma_o^2 = \frac{3\rho c}{\pi r_o^2 t_o} kE_T$$

where the seismic efficiency factor k ($=E_S/E_T$) has been introduced. As a conservative estimate, the time length, t_o, of the pulse is assumed to be the time of basin formation, and, for an upper limit for σ_o, the pulse length, r_o, may be approximated more closely by the size of the projectile. Gault et al. (1968) estimate that the time of crater formation scales as the square root of crater radius, and using known times for impact craters formed in the laboratory this can be expressed by $t_o = 0.041\, r_o^{\frac{1}{2}}$ where r_o is in cm. To first approximation, r_o is calculated by the scaling equation for craters larger than 1 km (Gault, 1974). Thus the maximum initial stress becomes (c.g.s.):

(3) $$\sigma_o^2 = \frac{73\rho c}{\pi}\left[\frac{1}{(.0135)}\ \frac{\rho^{\frac{1}{2}}}{\rho_p^{\frac{1}{6}}}\right]^{3.6} r_o^{1.1} k$$

where ρ and ρ_p are the densities of the target and projectile, respectively.

Reflection of the normally incident P wave from a free surface will accelerate the surface to a velocity $2\sigma/\rho c$. Using this velocity to estimate the total displacement (d) of a free surface particle under the gravitational acceleration (g) and incorporating the fact that elastic waves decrease inversely with the distance, r, we obtain the surface displacement in terms

of basin diameter ($D = 2r_o$):

(4) $$d = a\ k\ D^{3.1}$$

where

(5) $$a = \frac{17.5}{\pi g \rho c r^2} \left[\frac{1}{(.0135)} \frac{\rho^{1/2}}{\rho_p^{1/6}} \right]^{3.6}$$

Figure 3 shows displacements for antipodal points on the Moon for different values of k and D with assumed values of ρ, ρ_p, and c as 3.3 g/cm^3, 3.0 g/cm^3 and 8 km/sec, respectively (curves A_1, A_2, A_3). An incipient (premodified) basin 600 km in diameter (Imbrium ?) is indicated to produce a 1.7 m displacement for the seismic energy of $10^{-4} E_T$. Figure 3 (curve B) also shows calculated displacements using Baldwin's (1963) relation between crater diameter and total impact energy (c.g.s.) for large craters, $E = 2.394 \times 10^9 D^{3.05}$. For the given parameters and model, Baldwin's relation provides a lower limit on the calculated displacements. As noted above, an upper limit to the calculations results when the wavelength is assumed to be equal to the projectile diameter. The projectile diameter can be derived from the relation between the incipient crater diameter and total projectile energy, provided that the projectile velocity and density are assumed. For an impact velocity of 10 km/sec and projectile density 3 g/cm^3, Gault's relation, which was used in equation (3), yields an additional curve in Figure 3 (curve A_2').

A second independent calculation of antipodal displacement may be made from a different model derived by Jeffreys (Bullen, 1963, pp. 75-76). Rather than assuming an idealized shape of the impact-generated pulse, we can assume a source function that theoretically determines the pulse. In particular, a dilational wave is produced by an instantaneously and symmetrically applied pressure, σ_o, to a sphere of radius, a, inside a given medium. For Poisson's ratio equal to 0.25, the radial displacement produced by the

resulting wave from the center of the sphere is given by the following solution of the differential equation for large distances, r:

$$y = \frac{3\sqrt{2}\sigma_o a^2}{4\rho c^2 r} e^{-x/\sqrt{2}} \sin x \tag{6}$$

where

$$x = \frac{2\sqrt{2}\, c\, \Delta t}{3a} \tag{7}$$

and Δt is the time after the arrival of the wave. The initial pressure is calculated by assuming that the seismic energy is released as a linearly decreasing function of time, reaching a maximum at t = o and going to zero at t_o. Thus the total seismic energy released, kE_T, is simply $2t_o E_{so}$ where E_{so} represents the maximum seismic energy released at time t = o. It is assumed that the seismic energy is released at a distance, a, from the point of impact into a hemispherical shell of thickness Δs containing mass $2\pi a^2 \rho \Delta s$. Therefore, combining the Rankine-Hugoniot equations describing the conservation of energy and momentum for the passage of a shock wave, we obtain

$$\sigma_o^2 = \frac{2kE_T \rho c}{\pi a^2 t_o} \tag{8}$$

Thus, the radial displacement produced by the passage of the wave as a function of time parameter x becomes:

$$y = \frac{3}{2\sqrt{\pi}} \frac{a}{\rho^{1/2} c^{3/2} r} \left[\frac{kE_T}{t_o}\right]^{1/2} e^{-x/\sqrt{2}} \sin x \tag{9}$$

The maximum radial displacement, y_{max}, can be calculated by differentiating (9) with respect to time and maximizing the time dependent terms. A conservative estimate of the vertical "average" particle velocity is then calculated by dividing y_{max} by the time, Δt, it takes to reach this maximum displacement. The velocity of the free surface will be twice the particle velocity, and this velocity is used to calculate the maximum displacement, d, of a

free surface particle under lunar gravity. After incorporating Gault's scaling equation between energy and crater diameter, the resulting expression for d is the same as that described by equations (4) and (5) except for an additional factor

(10) $$\frac{4}{6}\,\frac{\sin^2 x}{x^2}\,e^{-x\sqrt{2}}$$

that has a numerical value of 0.126 at y_{max}.

Figure 3 shows two relations between displacement and the incipient crater diameter that result from this approach for lunar events. The higher values (curve C′) are obtained by assuming that the radius of the source hemisphere is the diameter of the projectile as derived from Gault's scaling equation, in which projectile velocity is 10 km/sec and projectile density is 3 g/cm^3. Lesser values (curve C) result from a source hemisphere the size of the incipient crater.

The important seismic efficiency factor (k) has been introduced in the foregoing calculations without discussion. Gault and Heitowit (1963) estimated from small-scale impact experiments that an upper limit of 10^{-2} of the projectile kinetic energy (E_T) will be partitioned into seismic waves for an impact in solid basalt. McGarr et al. (1969), however, calculated that for impacts into a bonded sand, the seismic energy represents only $6 \times 10^{-4}\ E_T$. Latham et al. (1970a) derived values of $10^{-5} E_T$ from missile impacts at the White Sands Missile Range and 10^{-6} to 10^{-5} for the Apollo 12 LM impact (Latham et al., 1970b). Consequently, a small impact (10^{16} ergs) into the lunar regolith will generate only meager seismic waves. However, a basin-sized impact (greater than 10^{30} ergs) will produce an enormous amount of seismic energy (E_S) not only due to the large E_T but also because the impact will penetrate deep into the lunar crust, thereby increasing E_S/E_T relative to the LM and missile impact data. Thus, an adopted value of $k = 10^{-4}$ represents a reasonable, if not conservative, approximation.

For an Imbrium-size basin (600 km diameter), Figure 3 indicates displacements from approximately 0.1 m to 20 m,depending on the accepted scaling relation, seismic model, and seismic efficiency. Baldwin's scaling relation is based on the final - not the incipient - basin diameter, which for Imbrium is approximately 1000 km. Consequently, the inferred kinetic energy is essentially the same (10^{34} ergs) as that from Gault's scaling relation, and curve (B) in Figure 3 will shift to the left near curve (A_2). The two approaches using the saw-toothed wave from Rinehart (curve A_2) and the source function from Bullen (curve C) are in better agreement than what is indicated by equation (10). If the particle velocity at time $\Delta t = 0$ is derived from differentiating equation (10), instead of approximating an "average" velocity, the resulting surface displacement is 0.7 that predicted by using the saw-toothed wave, thereby moving curve (C) towards curve (A_2). Thus it appears that the remaining differences in calculated surface displacements depend on the partition of the kinetic energy into seismic energy with respect to time (t_c) and position (r_o) as well as the overall seismic efficiency. As noted above, partitioning the seismic energy over a time equal to that for basin formation with an effective hemisphere of radius equal to that of the incipient basin has been shown to be a conservative approximation. Moreover, a seismic efficiency of 10^{-4} is a reasonable value based on experimental data. Therefore, vertical surface displacements between 2 m and 20 m appear to be a reasonable estimate.

Away from the antipodal point, the P wave will strike the surface obliquely, resulting in a reflected tensile wave and a shear wave. The division of energy into these waves is expressed by (see Rinehart, 1960, 1968):

(11)
$$\sigma' = R\sigma \quad \text{(tensile wave)}$$

(12)
$$\tau = (1+R)(\cot 2\beta)\sigma \quad \text{(shear wave)}$$

where β is the angle of reflection of the shear wave (from surface normal) and can be given in terms of either Poisson's ratio, ν, or the angle of incidence, α, where $\sin\beta = (c_s/c_p)\sin\alpha$. The factor R is the reflection coefficient:

(13) $$R = \frac{\tan\beta \tan^2 2\beta - \tan\alpha}{\tan\beta \tan^2 2\beta + \tan\alpha}$$

The displacement of the surface is determined by the sum of the component displacements from the impinging P wave, the reflected tensile wave, and the generated shear wave.

Figure 4 illustrates the component velocities for a 600 km diameter basin calculated from equations (3), (11), and (13) with $E_s = 10^{-4}E_T$ and Poisson's ratio, $\nu = 0.25$. It is clear that near the basin a very large horizontal velocity component is experienced. The maximum vertical displacement at a distance 1200 km from the basin center can be calculated to be 2 m. For comparison, extreme extrapolation of data from Latham et al. (1970a) for low energy (10^{15} - 10^{16} ergs) missile impacts suggest vertical ground movement of approximately 0.1 m. It should be noted, however, that the impact of the Apollo 13 SIV-B produced ground motion amplitude that was three orders of magnitude greater than that indicated by similar extrapolation.

The preceding calculations indicate that a lunar basin-forming impact of the order 10^{34} ergs may generate an antipodal seismic wave containing a compressive stress of several hundred bars. When the compressive wave reflects as a tensile wave at the basin antipode, the tensile stress will exceed the tensile strength of most common rock and will lead to spallation. A solid body with an emerging saw-toothed tensile wave will spall with a thickness $(\sigma_c/\sigma)(\lambda/2)$ and velocity $(2\sigma - \sigma_c)/\rho c$ where σ_c is the tensile strength of the material (Rinehart, 1960). Thus, for a homogeneously solid body the size of the Moon (a gross simplification) the formation of a 600 km incipient diameter basin

(Imbrium) would produce an antipodal spall of thickness 110 km and velocity 1.5 m/sec. Although gravity loading at such depths will raise the tensile strength and perhaps prevent actual spallation, pre-existing joints and crustal fractures should encourage failure.

An emerging P-wave near the source may be trapped in an early lunar or Mercurian crust and transmitted as a surface wave. Perhaps more importantly, during basin formation a significant portion of the seismic energy will be carried initially as surface waves (Love and Rayleigh waves). Only the mass elements below the basin will experience the high-velocity P waves that eventually reach the antipodal point. Because the surface waves geometrically disperse only as $r^{-\frac{1}{2}}$, they should produce a catastrophic jostling of the upper lunar crust out to large distances from the point of impact.

The magnitude of the Rayleigh wave can be estimated from an approximation made by Jeffreys and described by Bullen (1963). Specifically, the total energy per unit lunar surface area can be given by $16.8\,\pi\rho a^2 c^2/\lambda$ where ρ is the density of the upper lunar crust, the term a is a constant determining the amplitude of the surface wave near the source, c is the wave velocity, and λ is the wavelength. A conservative estimate of the seismic energy (E_{sr}) transmitted as surface waves can be made by assuming it to be the fraction of the area of the hemisphere described by the incipient basin of radius R ($A = 2\pi R^2$) that is represented by a surface layer of thickness H ($A = 2\pi RH$); i.e., the total energy of the surface waves is H/R that of the total seismic energy (E_s). This is a conservative estimate because a large amount of the total seismic energy will be spent in the early stage of crater formation when the projectile has not penetrated beneath this layer. Following Bullen, we can approximate λ to be the thickness of an "equivalent layer" which is assumed to be H. For a 600 km diameter excavation basin ($E_s = 10^{30}$, H = 25 km, $\rho = 3\,g/cm^3$, and c = 1.2 km/sec) this approximation indicates that the quantity

a is approximately 3 m. The maximum vertical lunar ground displacement corresponds to 2(.62)a, or approximately 4 m. For comparison, application of this approach to the missile impact data of Latham et al. (1970a) indicates theoretical Rayleigh wave amplitudes 2×10^{-2} less than the observed amplitudes. Consequently, major basin-induced displacements on the Moon on the order of 10 m are probably a conservative estimate.

Discussion of Results

The basic mechanics of spallation has been observed in the laboratory for small-scale impacts (Gault and Wedekind, 1969). Figure 5 illustrates the antipodal spallation of a glass sphere impacted by an aluminum sphere traveling at 0.95 km/sec. Although the impacted hemisphere and antipodal hemispheres exhibit extensive fracturing and spallation, the interior of the sphere remains relatively undamaged. It is important to note that antipodal spallation occurs regardless of the angle of impact (Figure 6). Pollack et al. (1972) give the binding energy of a strength-dominated body as $4\pi R^3 S/3$ where S is the strength and R is the radius. For the glass sphere shown in Figure 5, S is on the order of 10^9 dynes/cm^2 and the binding energy is therefore 2.7×10^{11}. The ratio of the energy of the projectile to this binding energy is 1×10^{-4} (for a glass sphere extensively shattered by an impact, this ratio is 0.25). A similar exercise can be made for a gravity-dominated body such as the Moon where the binding energy is the gravitational potential energy, or 1.2×10^{36} ergs. Consequently, the ratio of the kinetic energy of a projectile responsible for a 600 km diameter basin (10^{34} ergs) to the lunar binding energy becomes 8×10^{-3}. The enormous dimensional differences between the laboratory and lunar basin-forming impacts preclude detailed comparisons and inferences; however, general comparisons suggest that the formation of a large basin produces significant effects other than those produced by ballistic ejecta.

There are two contributions to the stresses responsible for antipodal disruption. The reflected tensile wave from the antipodal free surface has been considered in the preceding calculations. Additionally, the reflected tensile waves from the nonantipodal regions described by equation (11) will converge along the axis between the body's center and the antipode. Figure 7 illustrates the case for a spherical wave generated on the surface of a sphere. Convergent and opposing tensile waves exceeding the tensile strength of the body will aid in ripping apart the interior antipodal region. Theoretically, converging spherical waves will increase in strength by a factor r_1/r_2 where r_1 is the distance between the point of reflection and the point of convergence and r_2 is the distance of the converging wave from the point of convergence (Rinehart, 1960). The singularity at $r_2 = 0$ results from oversimplification of a problem more complicated than divergence, but it does illustrate that this axial focusing of tensile stresses may be sufficient to create deep-seated fractures of a planetary interior antipodal to a major basin.

Antipodal convergence of surface waves also should produce significant surface disruption from the formation of a major basin. With no attenuation and complete symmetry, the magnitude of surface displacement should increase as $(r_1/r_2)^{\frac{1}{2}}$, where r_1 is one half the distance from the basin to the antipodal point (one fourth the lunar circumference and r_2 is the distance of the converging surface wave from the antipodal point. Consequently, antipodal surface displacement may be comparable to that adjacent to the basin.

In a "real" Moon, several important departures from the presented theoretical model will occur. First, it is reasonable to suspect that the Moon and Mercury exhibit a gradual increase in the rigidity, and therefore the P-wave velocity, with depth. The result is the well-known refraction of a ray path describing the wave; in particular, the wave will emerge closer to the surface. This refraction also results in P-wave arrivals more nearly normal to the surface, thereby increasing the vertical velocity component at the expense of the horizontal component.

Second, these calculations have neglected the effect of a major discontinuity in the interior of the Moon or Mercury. As on the Earth, such a transition will produce a shadow zone that exhibits reduced effects of surface modification from the high-velocity body waves. This effect could be more pronounced on Mercury than on the Moon owing to the possibility that Mercury has an Fe-rich core (Murray et al., 1974).

Third, it has been assumed that no attenuation of the elastic wave occurs. Attenuation in the lunar crust has been found to be extremely low (Latham et al., 1972); therefore, its omission may not introduce serious error. However, surface waves performing work by their induced mass movement would be attenuated with increasing distance from the source, but such refinement is beyond the scope of the present study.

Fourth, the actual form of a seismic wave typically is not a single saw-toothed or sinelike wave; rather, it is a series of complex oscillatory ground movements resulting from wave dispersion within a heterogeneous body. This is known for the Earth (Bullen, 1963) and is particularly pronounced in the lunar seismic record for low-energy impacts (Latham et al., 1970b). However, the impulse produced by a basin-size impact is enormous relative to terrestrial and lunar seismic events, and it should retain its basic shape over greater distances. Moreover, a train of oscillatory waves containing this large seismic energy might be more damaging to surface structures than a single pulse owing to the rapid changes in acceleration. A detailed account of these effects is also beyond the scope of the order-of-magnitude calculations presented here.

Implications for Surface Processes

From the known effects of large earthquakes, Titley (1966) suggested that the seismic effects from relatively modest lunar impact events (10^{23} ergs)

would be shaking, compaction, and downslope mass movement. However, similar predictions of surface effects from seismic waves produced by enormous basin-forming impacts (10^{34} ergs) are highly speculative, but most certainly large-scale slope failure will occur. The competency of the upper lunar highland crust is low owing to a long history of impacts and ejecta deposition, and large craters within this terrain will be lined with scree slopes and relatively incompetent slumps. Old slumps might be reactivated by basin related seismic waves, but perhaps more frequently, debris slides and avalanches will furrow the old slump blocks. Consequently, large surface features could be modified heavily and in some cases morphologically rejuvenated. The intercrater regions, which have been blanketed by secondary ejecta from different sources, will exhibit modification produced by compaction and debris creep, and features with dimensions comparable to the wave-induced surface displacements should be erased. Resulting surface features could include subdued pits, hillocks, fractures, and chaotic textures.

In the interpretation of surface morphology, the arrival time of the seismic waves becomes an important consideration. Figure 8 shows the arrival times of ejecta, body waves, and surface waves for a 480 km diameter basin on the Moon. Such a basin approximately corresponds to the incipient Orientale Basin, the last major basin that remains relatively unaltered by subsequent basin formation and mare inundation. Because of basin size, the time and position of ejection have been included in the calculations and account for the nonlinearity in the times of ejecta arrival near the basin. Calculations were made for ejection angles between 60° and 30° from the surface normal, thereby bracketing the range of ejection angles deduced from small-scale impacts (Gault et al., 1963; Stöffler et al., 1974). Body waves in this illustration also exhibit nonlinearity, which expresses the radial body wave arrival at the surface of a sphere, whereas surface waves

describe a straight line. With the assumptions for basin formation, surface and body waves slower than approximately 1.2 km/sec will be partly consumed during crater formation if they are considered to originate at the center of the basin. More realistically, the seismic waves will originate at a distance comparable to the projectile radius, and Figure 8 shows the range of arrival times for a surface wave originating at the basin rim and one half the basin radius from the center.

From Figure 8, reasonable values of body waves (8 km/sec) indicate arrival at the lunar surface prior to any secondary ejecta. However, surface waves traveling at 1.2 km/sec, which is comparable to that observed for the Moon (Latham et al., 1970b), will arrive contemporaneously with the secondary ejecta at distances between 1200 km and 2000 km.

Ejecta arriving after the seismic waves will mask, in part, the seismic effects. This masking probably will be in the form of secondary craters and their tertiary ejecta. Extensive surface modification from severe seismic events, however, could remain evident as chaotic knobby terrains, large degraded crater walls, and perhaps radially trending structural features. Lower velocity surface waves will trail the ejecta beyond 1200 km, and this is approximately the range beyond which both craters with furrowed, subdued walls and the high-albedo plains units typically occur. Consequently, it is proposed that these features may be expressions of seismically induced mass movement of both old pre-existing topography and newly arrived secondary ejecta and their products. The passage of the surface wave probably was not a singular event but a complex train of ground movements that acted to "fluidize" the secondary and tertiary ejecta as well as the seismically induced landslides. In support of this interpretation, it is noted that the high-albedo plains units commonly occur within craters having furrowed walls

(Geber, Abulfeda) and within small localized depressions in hillocky terrains. Such short-term degradation is consistent with the preservation of small-scale surface features that are related to basin-forming events such as narrow (less than 0.5 km widths) patterned furrows and ridges in the inner basin ejecta facies of Orientale and Imbrium.

The most severe surface effects from seismic waves likely will occur where the waves encounter a relatively unconsolidated overlay. This is a common occurrence on the Earth, and the amplification of ground movement can be as great as a factor of 5 (Bolt, 1970). It is noted that the knobby and furrowed terrains that are not antipodal to a major and recent basin are found surrounding older basins. For example, the Sirsalis Rille region is adjacent to the old Humorum Basin. Similar terrains occur southeast of Humorum (near the crater Mercator), adjacent to the Nectaris Basin (near the Apollo 16 site and northeast of Nectaris), and around the Crisium Basin (Mare Marginis region as well as other regions). Moreover, the extensive knobby terrain along the eastern border of Serenitatis exhibits larger scale modifications thought to be related to the Imbrium event. These are regions where the bulk ejecta deposits are the thickest, and such deposits represent a major unit of relatively incompetent material, conditions ideal for seismic amplifications. The formation of such terrains by the most recent basins (Imbrium and Orientale) seems more consistent with their state of preservation than assigning them to effects of the old, degraded basins around which they commonly occur. In addition, this explanation could account for the asymmetry of the knobby terrains around the most recent Imbrium and Orientale basins.

Thus far, discussions have focused on surficial effects. It has been noted that deep-seated fractures may result from converging tensile waves and spallation-like effects within the antipodal crust. These fractures may aid in understanding the distribution of the lunar maria in a belt encircling

the Moon in a great circle (Stuart-Alexander and Howard, 1970). The fractures that developed antipodal to Imbrium would have enhanced the shattered zone beneath the enormous farside basin recognized by Schultz (1972) and could have acted as conduits for farside regional mare flooding. The antipode to Orientale also exhibits a concentration of mare units that extend in a line normal to the great circumferential maria belt (Schultz, 1974), and the vents for these eruptions also may be related to antipodal crustal fracturing.

Concluding Remarks

Formation of large basins on the terrestrial planets must have generated large-scale seismic effects. Evidence for these effects are more apt to be preserved on the Moon and Mercury whose surfaces have remained relatively unaltered by fluvial and eolian erosional processes as well as the effects of a dynamic interior (i. e. Mars). Theoretical estimates indicate that the vertical surface displacement from P waves antipodal to an Imbrium-size basin on the Moon could have been on the order of 10 m. Such waves would arrive prior to any secondary ejecta. Reflected tensile waves will converge within the Moon beneath the basin antipode and could produce or enhance deep-seated crustal weaknesses. Moreover, surface waves on the order of 10 m would arrive after secondary ejecta beyond approximately 10^3 km from the basin center and would increase in magnitude as they converge at the antipode. Based on these calculations, therefore, we suggest the following interpretations of certain enigmatic surface features:

1. Antipodal furrowed terrains represent effects of large-scale mass movement generated by the direct P waves and the later convergence of surface waves;

2. Subdued furrowed walls of 20 km - 30 km craters surrounding recent basins were produced by large-scale surface waves that triggered slope failure in pre-existing craters and interacted with the deposition of concomitant secondary and tertiary ejecta;
3. Emplacement and leveling of light plains units occurred when contemporaneous arrival of basin-related ejecta and surface waves resulted in mass transfer to topographic lows and "fluidizing" the slide materials;
4. Knobby and pitted terrains around old basins are the result of extensive surface modification produced by the enhancement of seismic waves in ancient basin-related ejecta blankets.
5. Distribution of farside lunar maria may be related to the convergence of reflected tensile waves that produced antipodal fractures or enhanced pre-existing weaknesses, thereby providing links to the deep-seated farside mantle at a later epoch.

Acknowledgements

We appreciate and gratefully acknowledge the review and constructive comments by Patrick Cassen, Bruce Smith, Ronald Greeley, and Ray Reynolds. One of us (P.H.S.) appreciates the opportunity to perform this research during tenure as a National Research Council - NASA Resident Research Associate.

REFERENCES CITED

Baldwin, R. B.: The measure of the Moon, 488 pp., Univ. of Chicago Press, Chicago, 1963.

Bullen, K. E.: An introduction to the theory of seismology, 381 pp., Cambridge University Press, Cambridge, 1963.

Eggleton, R. E.; and C. H. Marshall: Notes on the Apenninian Series and pre-Imbrian stratigraphy in the vicinity of Mare Humorum and Mare Nubium. Astrogeol. Studies Semiann. Prog. Rept., February 1961 - August 1961, pt. A, 132-137, U.S. Geol. Survey open-file report, 1962.

Gault, D. E.: Impact cratering. In A primer in lunar geology, R. Greeley and P. Schultz, eds., 137-176, NASA TM-62, 359, July, 1974.

Gault, D.E.; and E. D. Heitowit: The partition of energy for hypervelocity impact craters formed in rock. In Proceedings of sixth hypervelocity impact symposium, vol. 2, 419-456, 1963.

Gault, D. E.; E. M. Shoemaker; and H. J. Moore: Spray ejected from the lunar surface by meteoroid impact, NASA TN D-1767, Ames Research Center, 1963.

Gault, D. E.; W. L. Quaide; and V. R. Oberbeck: Impact cratering mechanics and structures. In Shock metamorphism of natural materials, B. M. French and N. M. Short, eds., 87-99, Mono Book Corp., Baltimore, 1968.

Gault, D. E.; and J. A. Wedekind: The destruction of tektites by micro-meteoroid impact. J. Geophys. Res., vol. 74, 6780-6794, 1969.

Howard, K. A.; D. E. Wilhelms; and D. H. Scott: Lunar basin formation and highland stratigraphy. Preprint, April 12, 1974.

Latham, G. V.; W. C. McDonald; and H. J. Moore: Missile impacts as sources of seismic energy on the Moon. Science, vol. 168, 242-245, 1970a.

Latham, G.; M. Ewing; J. Dorman; F. Press; N. Toksoz; G. Sutton; R. Meissner; F. Duennebier; Y. Nakamura; R. Kovach; and M. Yates: Seismic data

from man-made impacts on the Moon. Science, vol. 170, 620-626, 1970b.

Latham, G. V.; M. Ewing; F. Press; G. Sutton; J. Dorman; Y. Nakamura, N. Toksoz; D. Lammlein; and F. Duennebier: Passive seismic experiment. In Apollo 16 Preliminary Science Report, NASA SP-315, 9:1 - 9:29, 1972.

McGarr, A.; G. V. Latham; and D. E. Gault: Meteoroid impacts as sources of seismicity on the Moon. J. Geophys. Res., v. 74, 5981-5994.

Moore, H. J.; C. A. Hodges; and D. H. Scott: Multiringed basins - illustrated by Orientale and associated features. In Proc. Fourth Lunar Sci. Conf., Geochim. Cosmochim. Acta (in press, 1974).

Murray, B. C.; M. J. S. Belton; G. E. Danielson; M. E. Davies; D. E. Gault; B. Hapke; B. O'Leary; R. G. Strom; V. Suomi; N. Trask: Mercury's Surface: preliminary description and interpretation from Mariner 10 pictures. Science, vol. 185, 169-179, 1974.

Pollack, J. B. ; J. Veverka; M. Noland; C. Sagan; W. K. Hartmann; T. C. Duxbury; G. H. Born; D. J. Milton; and B. A. Smith: Mariner 9 television observations of Phobos and Deimos, Icarus, vol. 17, 394. 1972.

Rinehart, J. S.: On fractures caused by explosions and impacts. Quarterly of the Colorado School of Mines, vol. 55, No. 4, 155 pp., Goldon, 1960.

Rinehart, J. S.: Intense destructive stresses resulting from stress wave interactions. In Shock metamorphism of natural materials, B. M. French and N. M. Short, eds., 31-42, Mono Book Corp., Baltimore, 1968.

Schultz, P. H.: A preliminary morphologic study of the lunar surface. 967 pp. PhD thesis, University of Texas at Austin, August, 1972.

Schultz, P. H.: Moon morphology. University of Texas Press, Austin (in press) 1974.

Stöffler, D.; D. E. Gault; J. Wedekind; and G. Polkowski: Experimental hypervelocity impact into quartz sand: distribution and shock metamorphism of ejecta. Submitted to J. Geophys. Research, July 1974.

Stuart-Alexander, D. E.; and K. E. Howard: Lunar maria and circular basins -- a review, Icarus, vol. 12, 440-456, 1970.

Titley, S. R.; Seismic energy as an agent of morphologic modification on the Moon. In Astrogeol. Studies Ann. Prog. Rept. July 1, 1965 - July 1, 1966, pt. A, 87-103, U. S. Geol. Survey open-file report, 1966.

Titley, S. R.; and R. E. Eggleton: Description of an extensive hummocky deposit around the Humorum basin. In Astrogeol. Studies Ann. Prog. Rept.., July 1963 - July, 1964, pt. A, 85-89, U. S. Geol. Survey open-file report, 1964.

Trask, N. J.; and S. R.Titley: Geologic map of the Pitatus region of the Moon. U. S. Geol. Survey Misc. Geol. Inv. Map I-485, 1966.

Wilhems, D. E.; and J. F. McCauley: Geologic map of the near side of the Moon. U. S. Geol. Survey Misc. Geol. Inv. Map I-703, 1971.

Figure 1a: Mare Ingenii region on the Moon. The region shown is characterized by extensive grooves on the walls and rims of large craters; relatively smooth, subdued crater walls with only vestiges of slump blocks; hummocky and pitted intercrater areas; mare units that have embayed the modified crater interiors. This region is approximately antipodal to the Imbrium Basin. The bottom edge of the illustration corresponds to 350 km; north is to the bottom.

Figure 1b: Furrowed and pitted terrain adjacent to Mare Marginis on the Moon, a region approximately antipodal to the Orientale Basin. Large craters typically exhibit numerous wall furrows, subdued wall rubble, or large wall scarps. Two craters display central peaks surrounded by mare units (center) and light plains units (bottom). Intercrater regions are heavily pitted and grooved with complex surface textures. Unmodified craters with diameters larger than 15 km are sparse. Bottom edge of illustration corresponds to 350 km; north is to the bottom.

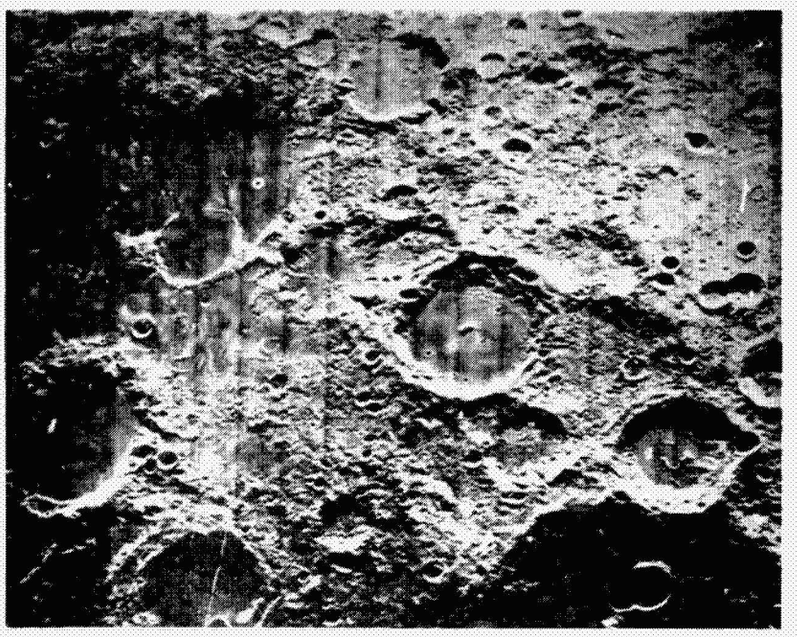

b

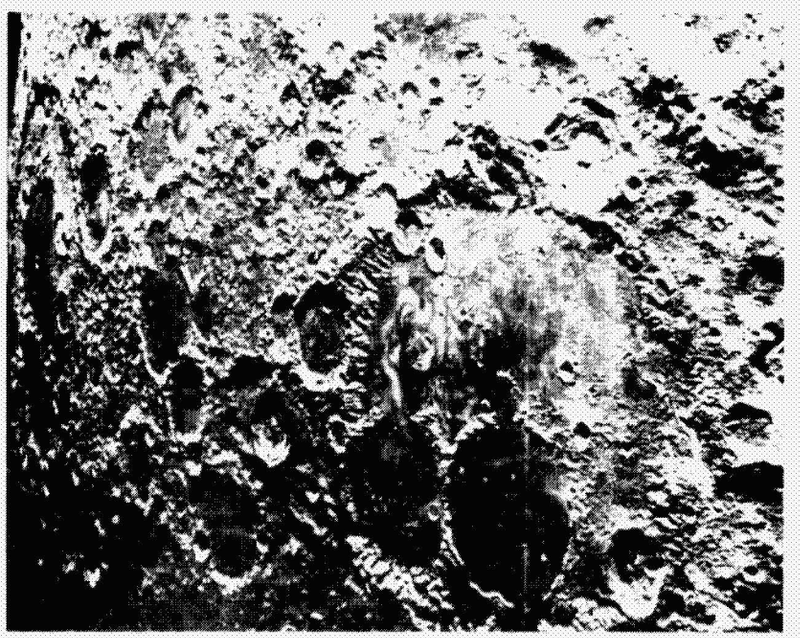

a

FIGURE 1

Figure 2: Hilly and lineated terrain antipodal to the Caloris Basin on Mercury. Large craters show extensive modification. Several display numerous subdued wall furrows (bottom) but exhibit preserved crested rim profiles. Plains units occur within shallow, modified craters. Intercrater regions are hillocky with transecting sets of NE- and NW-trending furrows. Bottom (north) of illustration corresponds to 350 km.

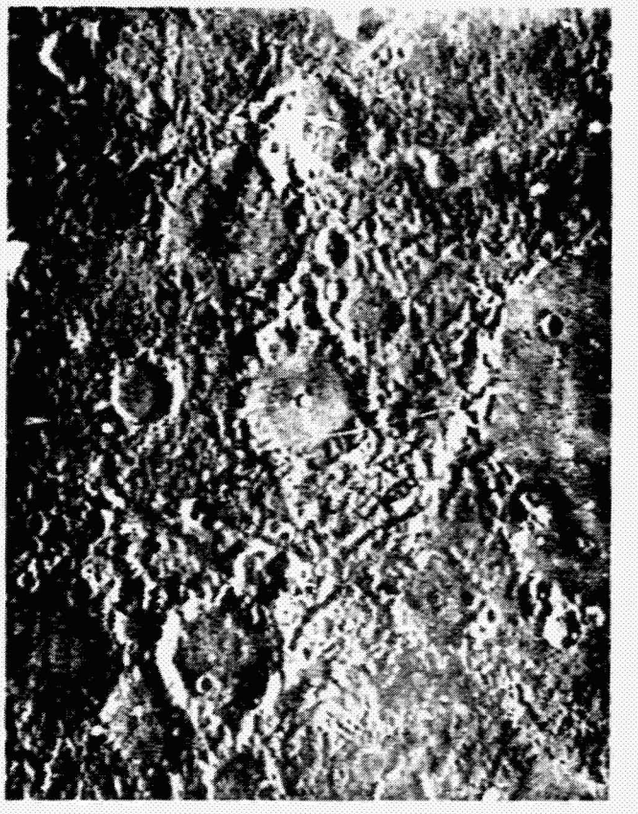

FIGURE 2

Figure 3: Calculated vertical surface displacements of the lunar surface antipodal to basins of different incipient (pre-slumping) diameters. The three relations A_1, A_2, and A_3 are based on sawtooth waves with scaling relation given by Gault (1974) and correspond, respectively, to seismic efficiencies (k) of 10^{-3}, 10^{-4}, and 10^{-5}. These curves incorporate a wavelength equal to the incipient basin diameter, whereas A_2' incorporates a wavelength equal to the projectile diameter (velocity 10 km/sec, density 3g/cm^3) for $k = 10^{-4}$. Relation B corresponds to A_2 ($k = 10^{-4}$) for a scaling relation given by Baldwin (1963). Curves C and C′ were derived from expressions given by Bullen (1963) with assumptions comparable to those for A_2 and A_2', respectively. Empirical relations relate the displacement, d (cm), seismic efficiency, k, and incipient basin diameter, D (cm).

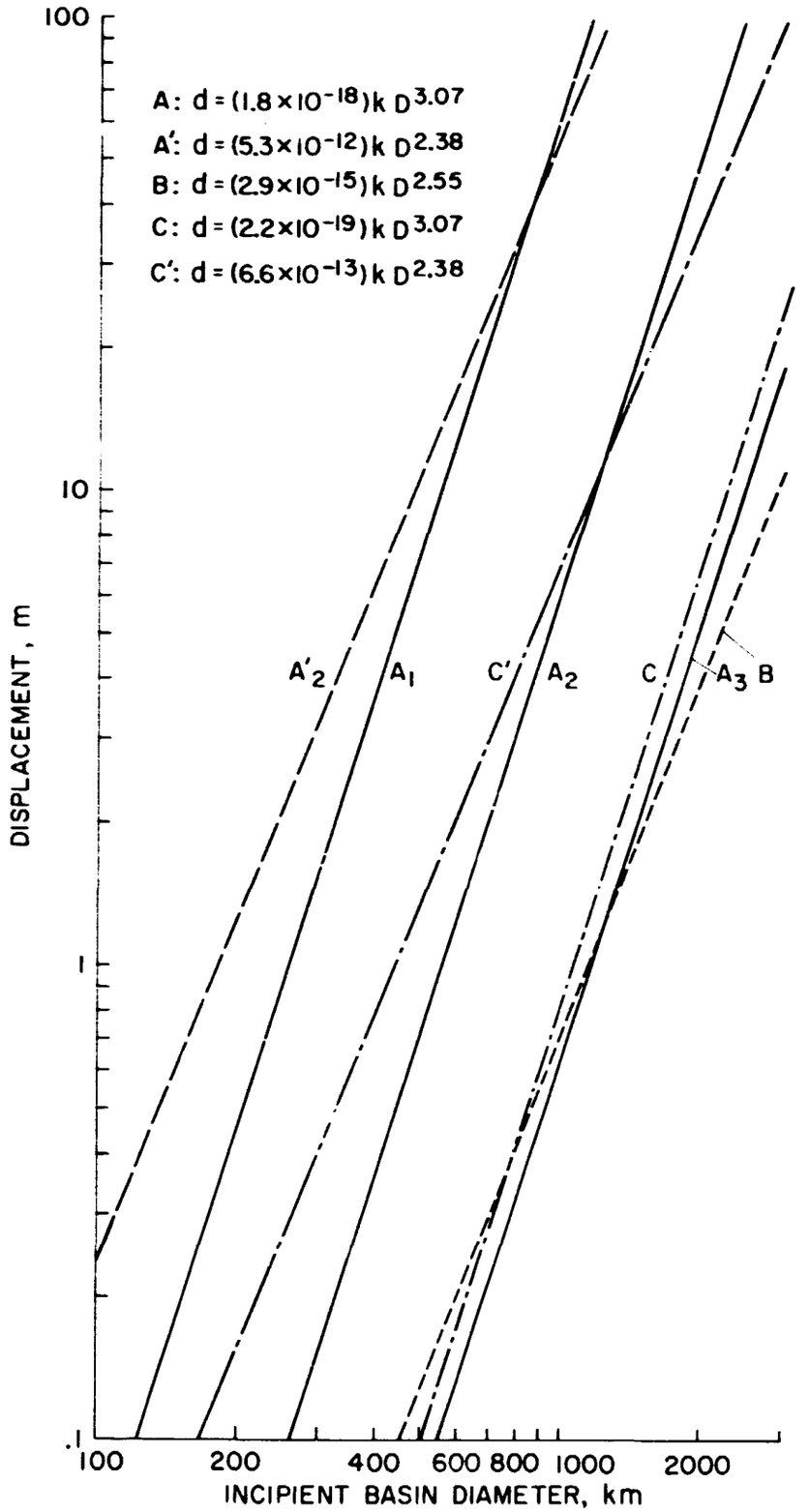
100
10
1
.1
A: d = (1.8×10⁻¹⁸)k D^3.07
A': d = (5.3×10⁻¹²)k D^2.38
B: d = (2.9×10⁻¹⁵)k D^2.55
C: d = (2.2×10⁻¹⁹)k D^3.07
C': d = (6.6×10⁻¹³)k D^2.38
A'2
A1
C'
A2
C
A3
B
DISPLACEMENT, m
100
200
400
600
800
1000
2000
INCIPIENT BASIN DIAMETER, km

Fig. 3

Figure 4: Vertical and horizontal particle velocities resulting from incident P-wave, reflected tensile wave, and generated shear wave at the lunar surface. Calculations are for a 600 km diameter incipient basin (Imbrium) and do not include wave refraction in the lunar interior. Arrow indicates the point antipodal to the basin.

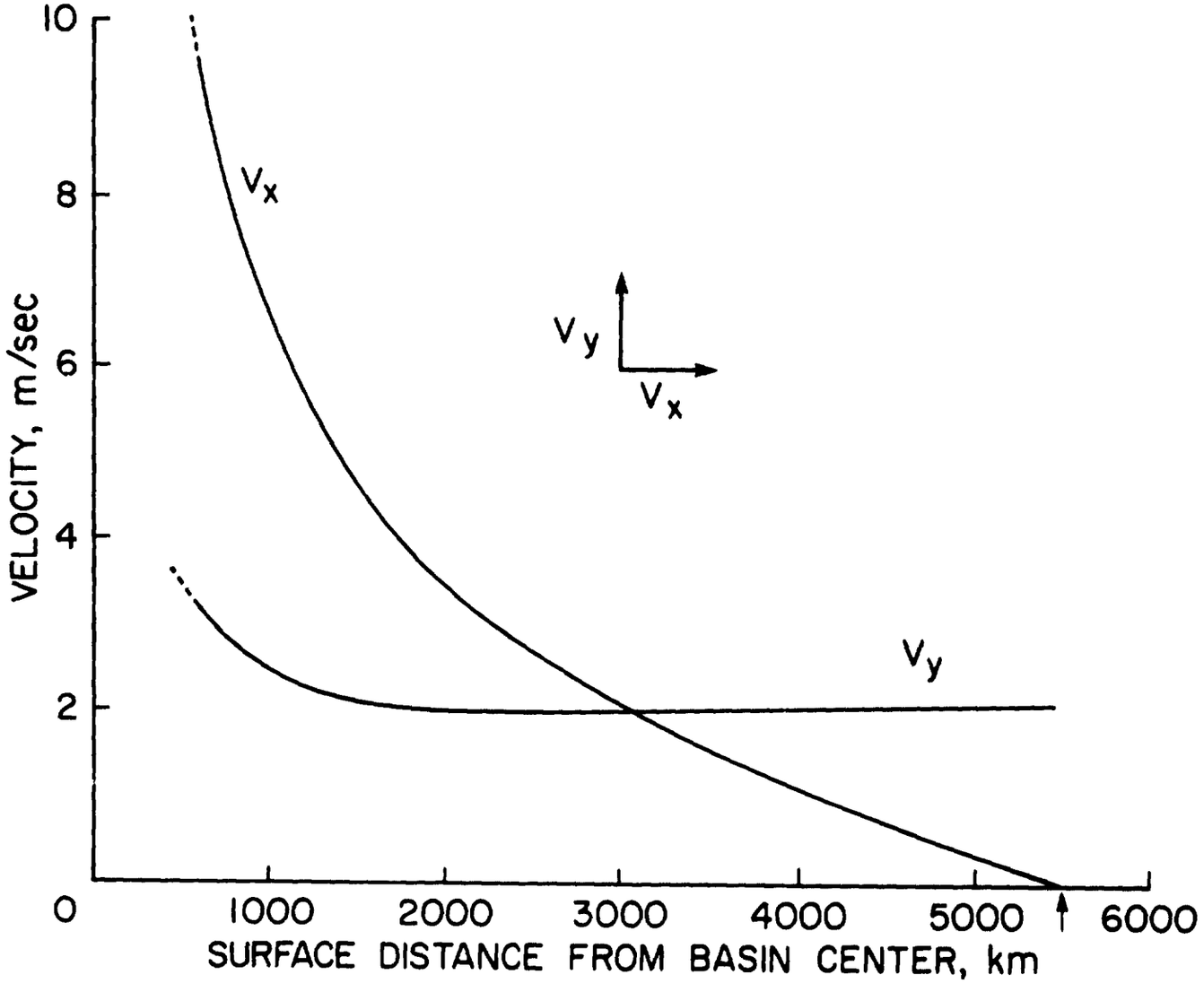
10
8
6
4
2
0
VELOCITY, m/sec
Vx
Vy
Vx
Vy
1000
2000
3000
4000
5000
6000
SURFACE DISTANCE FROM BASIN CENTER, km

Fig. 4

Figure 5: Impacted (right) and spallation (left) surfaces of a glass sphere 8 cm in diameter. Impacting projectile was a 1.59 mm diameter aluminum sphere traveling at 0.95 km/sec.

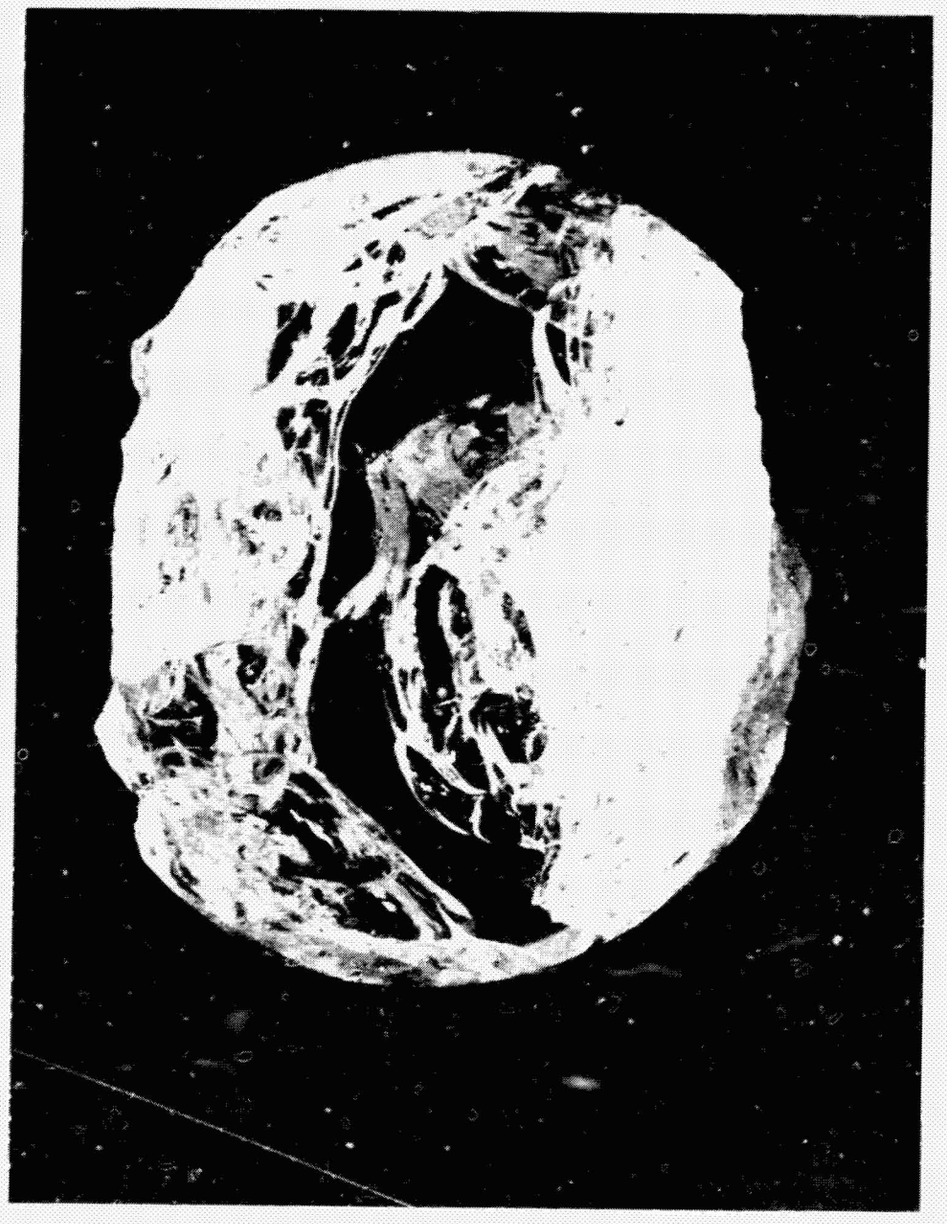

FIGURE 5

Figure 6: Antipodal spallation of a glass sphere (4.6 cm in diameter) produced by an impacting aluminum sphere (3.17 mm in diameter) at 2.31 km/sec from the right. Frames from a high-speed framing camera are shown for times in milliseconds from impact. Modified from Gault and Wedekind (1969).

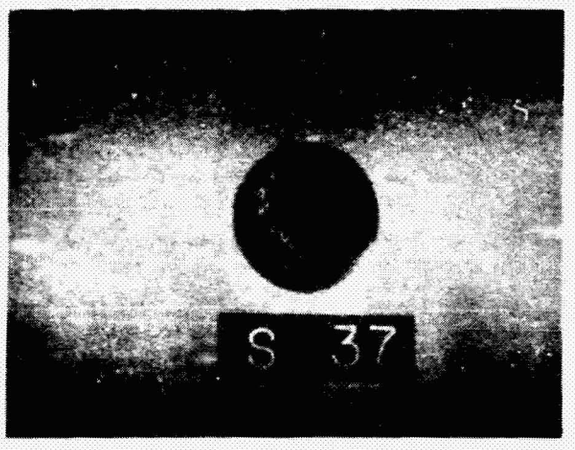

IMPACT

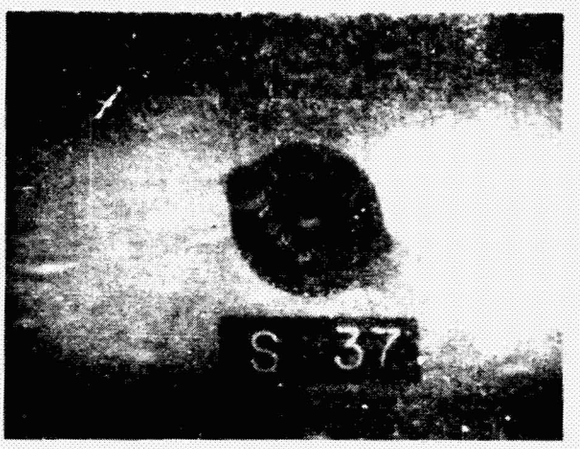

0.13

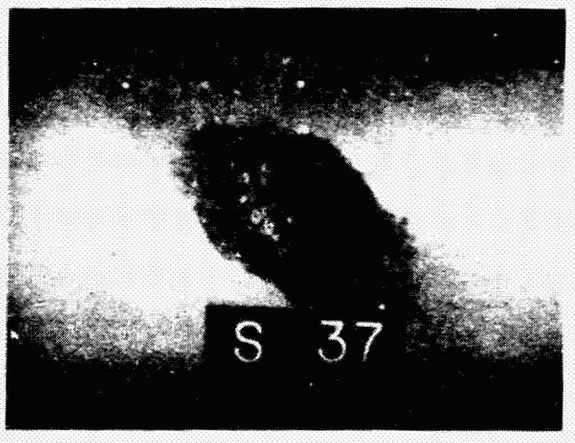

0.75

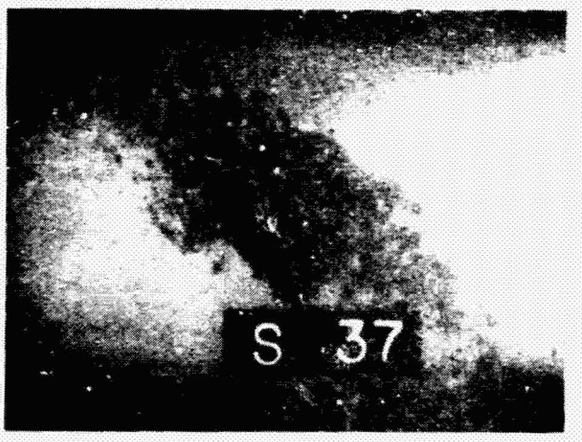

2.38

12.1

30.5

Figure 7: Convergence of tensile stresses in a spherical body from a spherical wave generated at the surface. At impact (A), compressive wave (solid line) is generated that develops a train of reflected tensile waves (dotted lines, B). Tensile wave front (C) is composed of reflected tensile waves from different portions of the lunar surface at different times, thereby producing a curved wave front containing different directions of propagation (arrows). Antipodal tensile wave (D) rapidly propagates inward, and the components reflected at greater distances from the antipode converge along the basin-antipode axis at progressively greater angles with respect to each other, ultimately resulting in opposing tensile stresses (E, F). Modified from Rinehart (1960).

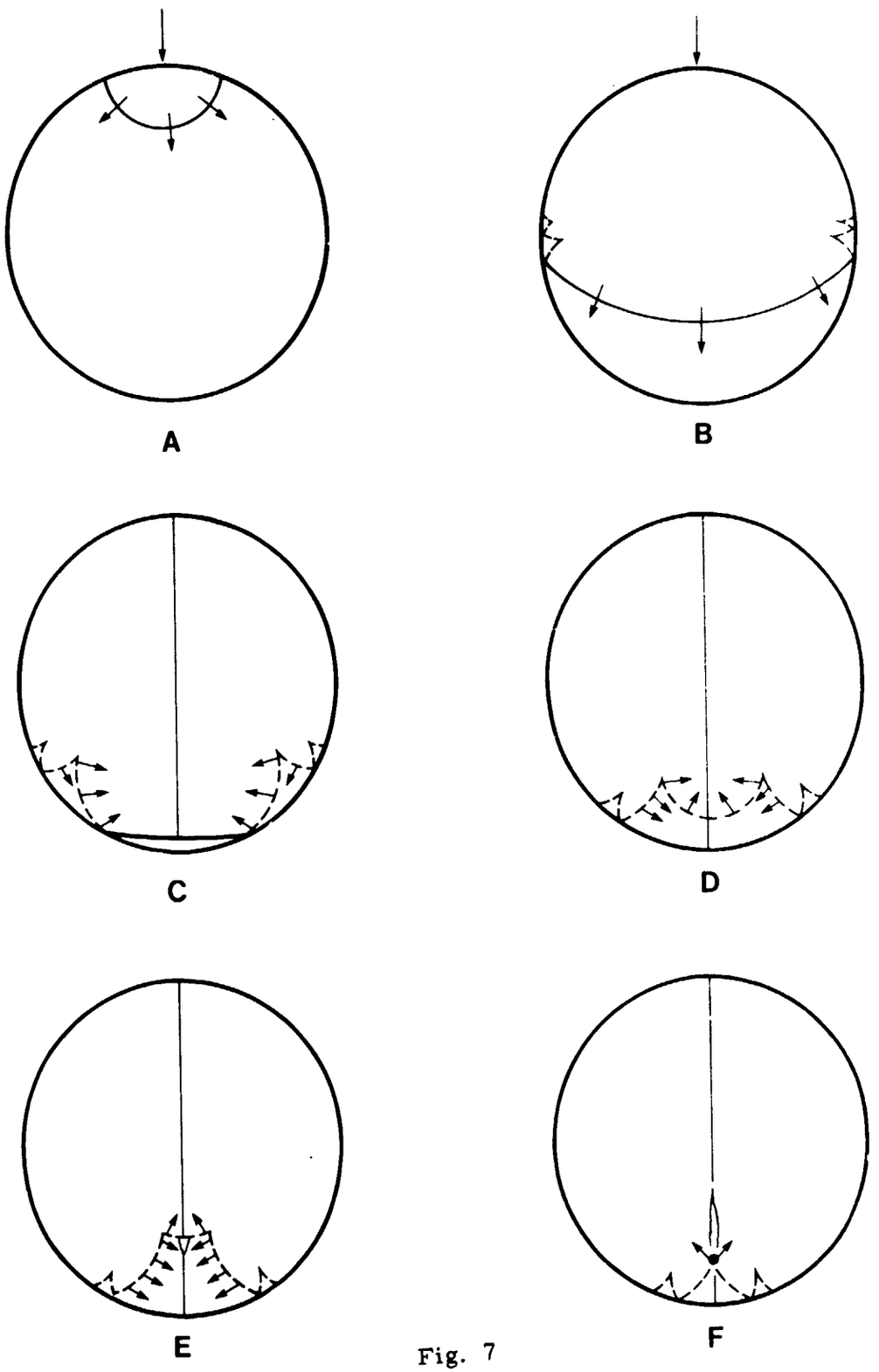

Fig. 7

Figure 8: Comparison between arrival times of body waves, surface waves, and secondary ejecta from a 480 km diameter lunar basin (Orientale). Arrival times of ejecta allow for the finite time of basin formation and changing position of ejection. Specifically, the time of ejection is assumed to be a linear function of velocity between 0 km/sec and 2.3 km/sec, and the developing crater is assumed to enlarge linearly with time after 0.3 minutes until the transient basin is complete (3.3 minutes). The vertically hatchured region indicates the range of possible ejecta arrival times dependent on ejection angle (β) from the surface normal and velocity. Arrival time of the surface wave is bracketed by two possible points of origin: basin radius and one half the basin radius.

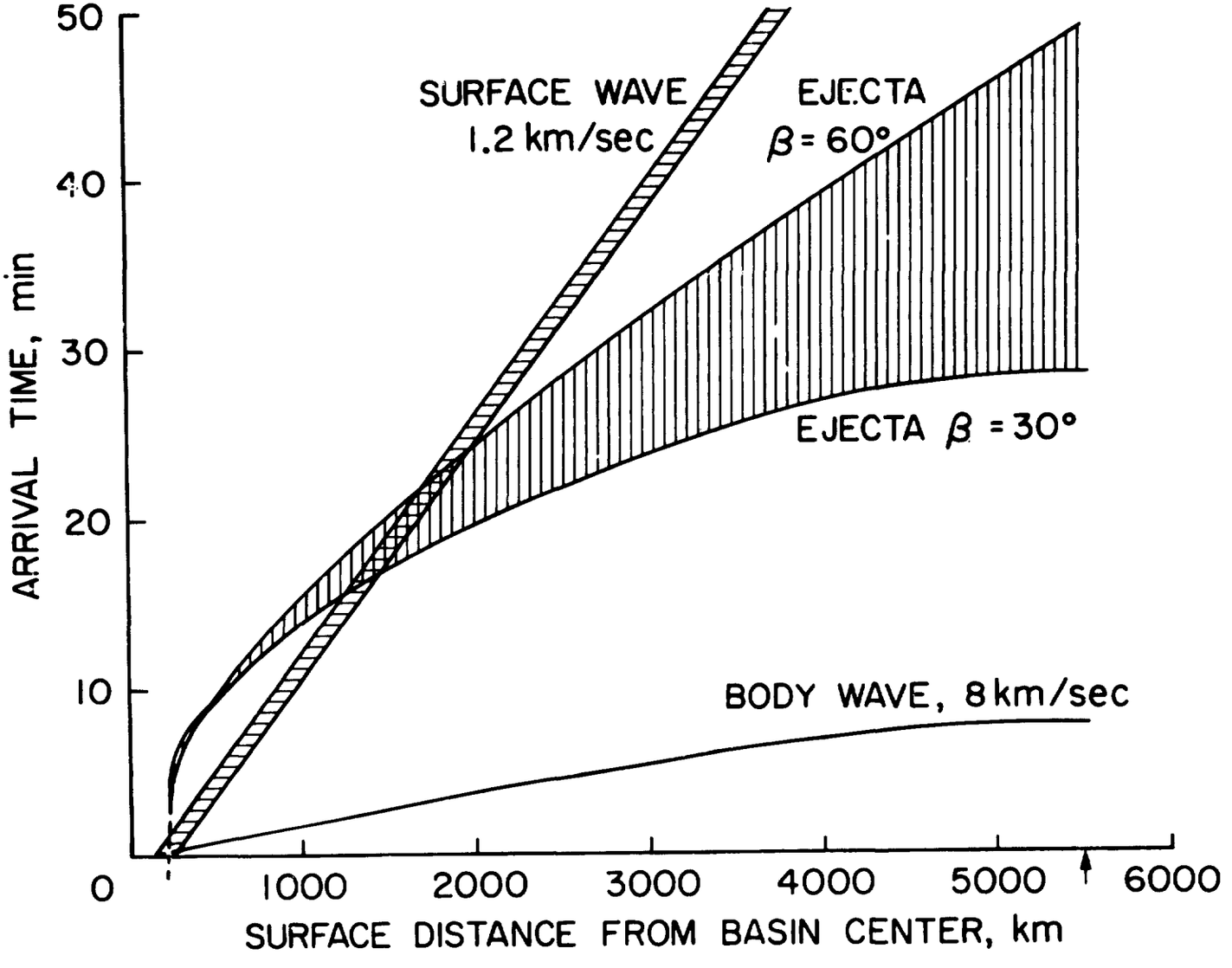
50
40
30
20
10
0
ARRIVAL TIME, min
SURFACE WAVE
1.2 km/sec
EJECTA
β = 60°
EJECTA β = 30°
BODY WAVE, 8 km/sec
1000
2000
3000
4000
5000
6000
SURFACE DISTANCE FROM BASIN CENTER, km

Fig. 8